

# Stability, structure, and oxidation state of Mo/H-ZSM-5 catalysts during reactions of CH<sub>4</sub> and CH<sub>4</sub>–CO<sub>2</sub> mixtures

Howard S. Lacheen, Enrique Iglesia \*

*Department of Chemical Engineering, University of California at Berkeley, Berkeley, CA 94720, USA*

Received 1 October 2004; revised 25 November 2004; accepted 29 November 2004

## Abstract

Mo<sub>2</sub>O<sub>5</sub><sup>2+</sup>-ZSM-5 (Mo/Al<sub>f</sub> = 0.4, Si/Al<sub>f</sub> = 20) samples prepared by sublimation of MoO<sub>3</sub> were carburized in CH<sub>4</sub> to form MoC<sub>x</sub> clusters active in CH<sub>4</sub> pyrolysis and then exposed to different CO<sub>2</sub>/CH<sub>4</sub> mixtures. CO<sub>2</sub>/CH<sub>4</sub> reactant ratios between 0 and 0.1 increased catalyst stability but decreased pyrolysis rates, and ratios above 0.1 led to a sudden loss of activity that was reversed after removal of CO<sub>2</sub>. Below CO<sub>2</sub>/CH<sub>4</sub> ratios of 0.1, the catalyst bed can be described as a CO<sub>2</sub>-reforming and pyrolysis reactor in series. In the first segment of the bed, where CO<sub>2</sub> is present, pyrolysis is completely suppressed by reverse Boudouard reactions; pyrolysis reactions begin after CO<sub>2</sub> is completely consumed. CO<sub>2</sub> cannot directly influence rates or deactivation for pyrolysis reactions. Rather, the greater stability observed with CO<sub>2</sub>-containing reactants arises solely from the presence of H<sub>2</sub>, formed in the CO<sub>2</sub>-reforming section, in the pyrolysis regions within the catalyst bed. The evolution of catalyst structure and composition in CO<sub>2</sub>/CH<sub>4</sub> reactants was also probed by mass spectrometric analysis of effluent streams and by in situ X-ray absorption spectroscopy to determine the underlying processes responsible for reversible deactivation at CO<sub>2</sub>/CH<sub>4</sub> ratios greater than 0.1. MoC<sub>x</sub>-ZSM-5 samples exposed to CO<sub>2</sub>/CH<sub>4</sub> streams with 0.022 and 0.055 ratios at 950 K acquire 0.3 ± 0.01 and 1.75 ± 0.03 O-atoms/Mo, respectively. X-ray absorption edge energies in MoC<sub>x</sub>-ZSM-5 increased from 0.2 to 1.9 eV (relative to Mo<sup>0</sup>) after contact with 0.025 CO<sub>2</sub>/CH<sub>4</sub> mixtures at 950 K for 1 h, indicating that oxidation of some Mo centers occurs. These spectral changes occurred concurrently with the detection of pre-edge features typical of MoO<sub>x</sub> structures. Radial structure functions resemble those for samples exposed to pure CH<sub>4</sub>, which consist of 0.6-nm MoC<sub>x</sub> clusters, but show an additional Mo–O coordination shell also detected in bulk β-Mo<sub>2</sub>C exposed to ambient air. These data suggest that the inhibition and ultimate suppression of catalytic pyrolysis reactions with CO<sub>2</sub> addition reflect the oxidation of active MoC<sub>x</sub> structures, the extent of which increases with increasing CO<sub>2</sub>/CH<sub>4</sub> reactant ratios. CO<sub>2</sub>/CH<sub>4</sub> reactant ratios above 0.1 lead to conversion of MoC<sub>x</sub> to MoO<sub>x</sub> structures, which are inactive for both reforming and pyrolysis reactions of CH<sub>4</sub>, but which reform active MoC<sub>x</sub> after an induction period when exposed to pure CH<sub>4</sub> reactants at reaction conditions.

© 2004 Elsevier Inc. All rights reserved.

*Keywords:* Molybdenum; Carbides; ZSM-5; MFI; CO<sub>2</sub>; CH<sub>4</sub>; Reforming; Pyrolysis; EXAFS; XANES; Aromatization

## 1. Introduction

Medium-pore zeolites with MFI structure and modified by transition metal cations catalyze oligomerization, cyclization, and dehydrogenation reactions required to convert small alkanes to alkenes and arenes [1–14]. Wang et al. [15] first reported that MFI modification by contact with aqueous Mo<sup>6+</sup> salts leads to near-equilibrium yields of ethene,

ethane, and benzene during nonoxidative CH<sub>4</sub> reactions with low selectivities for larger unsaturated products, apparently because of steric constraints imposed by MFI channels. MoO<sub>x</sub> precursors were shown to form carbide clusters during initial contact with CH<sub>4</sub> at 950 K [16]; these clusters provide the catalytic surfaces required for activation of C–H bonds in CH<sub>4</sub> and for removal of H-atoms as H<sub>2</sub> during both CH<sub>4</sub> conversion to C<sub>2</sub> molecules and sequential conversion of these primary C<sub>2</sub> products to arenes [17]. The exchange of acidic protons with D<sub>2</sub> [18], together with Raman spectroscopy and multiple-scattering simulations of the extended

\* Corresponding author.

E-mail address: [iglesia@cchem.berkeley.edu](mailto:iglesia@cchem.berkeley.edu) (E. Iglesia).

fine structure in X-ray absorption spectra [19], provided direct evidence that Mo(VI)-oxo dimers form at exchange sites during sublimation of MoO<sub>3</sub>/H-ZSM-5 physical mixtures. These Mo-oxo dimers subsequently convert to active MoC<sub>x</sub> structures during CH<sub>4</sub> reactions.

Mo-ZSM-5 catalysts deactivate during nonoxidative CH<sub>4</sub> reactions [20–22] via carbon deposition processes, which become slower as external acid sites on zeolite crystals are selectively titrated by bulky organosilanes [23]. CO<sub>2</sub>/CH<sub>4</sub> mixtures lead to slower deactivation than pure CH<sub>4</sub> reactants [24,25], an observation attributed to continuous carbon removal via



A sudden loss of catalytic activity above a threshold CO<sub>2</sub>/CH<sub>4</sub> reactant ratio (~0.06), reversed upon removal of CO<sub>2</sub> from the CH<sub>4</sub> reactant stream, has also been reported [26]. This sudden but reversible deactivation in CO<sub>2</sub>/CH<sub>4</sub> feeds appears to reflect the oxidation of MoC<sub>x</sub> instead of carbon deposition processes prevalent with pure CH<sub>4</sub> reactants [27]. At CO<sub>2</sub>/CH<sub>4</sub> ratios below these threshold values, CH<sub>4</sub> conversion rates were lower but more stable than those obtained with pure CH<sub>4</sub> reactants. These lower rates reflect, at least in part, kinetic and thermodynamic inhibition by H<sub>2</sub> formed in CH<sub>4</sub>–CO<sub>2</sub> reforming reactions; H<sub>2</sub> can also inhibit the formation of large organic residues. Lower pyrolysis rates may also reflect the continuous removal of reactive carbon, required for C–C bond formation, as CO, with the use of CO<sub>2</sub> as a reactant. Green et al. [28] examined CO<sub>2</sub> reforming on bulk Mo<sub>2</sub>C and WC and proposed that CO<sub>2</sub> dissociates at carbon vacancies to form a steady-state concentration of chemisorbed oxygen (O\*) at carbide surfaces. High O\* thermodynamic activities, prevalent at high CO<sub>2</sub>/CH<sub>4</sub> ratios, can lead to Mo<sub>2</sub>C oxidation to less reactive MoO<sub>x</sub> species.

Here we probe CH<sub>4</sub> pyrolysis catalysis and deactivation pathways on carburized Mo<sub>2</sub>O<sub>5</sub><sup>2+</sup>-ZSM-5 at low CO<sub>2</sub> concentrations by rigorously isolating and examining the kinetic and thermodynamic effects of CO<sub>2</sub> on measured reaction rates. Kinetic factors contributing to decreased hydrocarbon formation rates such as C\* scavenging by CO<sub>2</sub> and H<sub>2</sub> and oxidative deactivation of carbide active sites are examined independently with varying feed composition and concentration. In contrast to previous studies, we report true forward rates by accounting for reactions of products and using thermodynamic equations that account for the equilibrium approach inherent in measured rates. Moreover, we report new evidence suggesting that the enhanced stability of Mo-ZSM-5 in CO<sub>2</sub>/CH<sub>4</sub> mixtures is due to H<sub>2</sub> alone and not, as previously proposed, CO<sub>2</sub> [24]. Finally, in situ time-resolved mass spectrometry and X-ray absorption spectroscopy were used to measure the oxidation state, local coordination, and structure of Mo-ZSM-5 in CH<sub>4</sub> reactants with low CO<sub>2</sub> concentrations and to identify processes leading to the observed effects of CO<sub>2</sub> on the catalytic rates, selectivity, and ultimate reversible deactivation of active Mo-based structures at high CO<sub>2</sub> concentration.

## 2. Experimental

### 2.1. Catalyst synthesis

We prepared H-ZSM-5 from Na-ZSM-5 (Si/Al<sub>f</sub> = 20, Zeochem; Al<sub>f</sub> = framework Al) by heating Na-ZSM-5 (2 g) to 823 K at 0.083 K s<sup>-1</sup> in He (2.5 cm<sup>3</sup> s<sup>-1</sup> g<sup>-1</sup> Airgas, UHP) and holding at 823 K for 2 h in dry air (2.5 cm<sup>3</sup> s<sup>-1</sup> g<sup>-1</sup> Airgas, zero grade), a process that removes the organic templates used in ZSM-5 synthesis without a detectable loss of crystallinity. The resulting template-free Na-ZSM-5 (10 g) was converted to NH<sub>4</sub>-ZSM-5 by ion exchange with 1 L of NH<sub>4</sub>NO<sub>3,aq</sub> (1 M, Fisher, Cert. ACS) at 353 K for 12 h, followed by washing with 2 L of deionized H<sub>2</sub>O. This exchange procedure was carried out three times with fresh solutions; samples were then dried for 12 h at 400 K in ambient air. NH<sub>4</sub>-ZSM-5 (5 g) was converted to H-ZSM-5 by heating in 0.5 cm<sup>3</sup> s<sup>-1</sup> g<sup>-1</sup> dry air to 773 K at 0.167 K s<sup>-1</sup> and holding for 24 h. H-ZSM-5 and MoO<sub>3</sub> (Johnson Matthey, 99.5%) were then ground in an agate mortar and pestle for 0.2 h to form intimate mixtures containing a Mo/Al<sub>f</sub> ratio of 0.41. This mixture was heated to 623 K at 0.167 K s<sup>-1</sup> and then held at 623 K for 24 h in 20% O<sub>2</sub>/He to remove water and to spread MoO<sub>3</sub> on external zeolite surfaces [17,19]; finally, the mixture was heated to 973 K at 0.167 K s<sup>-1</sup> and held at 973 K for 2 h to form exchanged Mo<sub>2</sub>O<sub>5</sub><sup>2+</sup>-ZSM-5 [19]. The catalysts were formed into pellets with 0.12–0.25-mm diameter for use in structural characterization and catalytic studies.

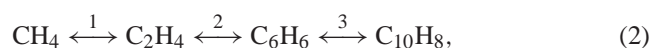
### 2.2. Catalytic reactions of CH<sub>4</sub> and CH<sub>4</sub>–CO<sub>2</sub> mixtures

Steady-state catalytic rates were measured at 950 K with 1-g catalyst samples held within a quartz reactor (12 mm i.d.). Reactants were 90% CH<sub>4</sub>/Ar (Matheson, UHP, purified with a Matheson MTRP-0019-XX oxygen-moisture trap; 1 bar total pressure, 0.208 cm<sup>3</sup> s<sup>-1</sup>) mixed with 50% CO<sub>2</sub>/He (Matheson, UHP) or H<sub>2</sub> (Airgas, UHP). We held CH<sub>4</sub> partial pressures constant (91 kPa) when using CO<sub>2</sub> or H<sub>2</sub> coreactants by increasing the total reactor pressure. The reactor effluent was directly transferred via heated lines (423 K) into a gas chromatograph (Agilent model 6890). Hydrocarbons were separated with a capillary column (Agilent HP-1, 50 m × 0.32 mm × 1.05 μm) and their concentrations were measured by flame ionization. CH<sub>4</sub>, Ar, CO, CO<sub>2</sub>, and H<sub>2</sub> were separated with a packed column (Agilent Porapak Q, 4.5 m) connected to a thermal conductivity detector. CH<sub>4</sub> conversion rates were measured with Ar as an internal standard to ensure rigorous mass balances. Product selectivities are reported on a carbon basis as the percentage of converted CH<sub>4</sub> molecules appearing as each product. Unreactive residues or nonvolatile products remaining on catalysts or transfer lines were determined by difference and reported as C<sub>12+</sub>. CO selectivities are reported as the percentage of the CH<sub>4</sub> converted and appearing as CO (using half the total CO formed, i.e., excluding CO formed in Eq. (1)); in this way,

the sum of all reported carbon selectivities, including CO, equals unity. Yields are reported as the product of each selectivity and the fractional CH<sub>4</sub> conversion.

Measurements of O-atoms removed from or added to the catalyst with sudden changes in reactant composition required product analyses at short time intervals (< 1 s). Product evolution rates in these experiments were measured by mass spectrometry (MKS Minilab with electron multiplier; detection limit  $\sim 1 \times 10^{-4}$  kPa for fixed gases), with the use of a heated capillary for continuous sampling of condensable species. All transient experiments were conducted at 950 K and ambient total pressure. During reduction/carburization of Mo<sub>2</sub>O<sub>5</sub><sup>2+</sup>-ZSM-5, the reactor feed was rapidly changed from pure He at 1 cm<sup>3</sup> s<sup>-1</sup> to a mixture containing 54 kPa CH<sub>4</sub>, 6 kPa Ar, and the balance in He at a total flow rate of 1 cm<sup>3</sup> s<sup>-1</sup>. During oxidation of reduced/carburized Mo-ZSM-5, the feed was switched from the latter composition to one containing 54 kPa CH<sub>4</sub>, 6 kPa Ar, 1–3 kPa CO<sub>2</sub>, and He as a balancing gas to maintain a constant flow of 1 cm<sup>3</sup> s<sup>-1</sup>. CH<sub>4</sub> pyrolysis and reforming products with overlapping mass fragments were measured with the use of matrix deconvolution methods adapted from earlier studies [18,29].

Measured net product formation rates are lower than the true kinetic forward rates when the product formed is involved in subsequent reactions or when reverse reactions become important near equilibrium. Forward rates,  $r_{\text{forward}}$ , corrected from the measured net reaction rates,  $r_{\text{net}}$ , in a sequential reaction (Eq. (2)) can be determined by correction for the approach to thermodynamic equilibrium with



$$r_{\text{C}_2\text{H}_4, \text{forward}} = r_{\text{C}_2\text{H}_4, \text{net}} + r_{-1} + r_{\text{C}_6\text{H}_6, \text{net}} + r_{\text{C}_{10}\text{H}_8, \text{net}}, \quad (3)$$

$$r_{\text{C}_2\text{H}_4, \text{net}} + r_{-1} = r_{\text{C}_2\text{H}_4, \text{net}} / (1 - \eta_1), \quad (4)$$

where the approach to equilibrium for reaction  $j$ ,  $\eta_j$  (where  $j = 1$  for ethene formation from methane), is given in terms of the partial pressures (in atm),  $p_i$ , of chemical species,  $i$ , and the equilibrium constant,  $K_j$ , for each reaction [30]

$$\eta_j = \frac{p_{\text{C}_2\text{H}_4}^{1/2} p_{\text{H}_2}}{p_{\text{CH}_4} K_j}. \quad (5)$$

### 2.3. Mo K-edge X-ray absorption spectroscopy

X-ray absorption spectra (XAS) were measured with the use of beamline 4-1 at the Stanford Synchrotron Radiation Laboratory (SSRL). Spectra were recorded in transmission mode with the use of three ionization chambers in series filled with a constant Ar flow. Catalyst samples were placed between the first two detectors, and a Mo foil (2.5  $\mu\text{m}$ ) was placed between the last two. The energy scale was calibrated from the first inflection point in the Mo foil K-edge (20 keV). The beamline was equipped with a Si(220) double-crystal monochromator and a downstream horizontal aperture (0.2 mm  $\times$  5.0 mm). Signal intensities were detuned to

70% of their maximum levels to minimize harmonic contributions. Spectra were acquired in 5-eV increments within the pre-edge region (19.80–19.98 keV), 0.25 eV near the edge (19.98–20.04 keV), and 0.04  $\text{\AA}^{-1}$  in the fine structure region (3.24–16 k). Transient experiments required rapid scanning for accurate assessments of the dynamic evolution in the near-edge spectra (< 1 ks per spectrum). These rapid scans were measured in 5-eV increments from 19.85 to 19.98 keV, 0.5 eV from 19.98 to 20.03 keV, 3.77 eV from 20.03 to 20.13 keV, and 20.4 eV from 20.13 to 20.73 keV. The two types of spectral acquisition protocols described above are hereinafter denoted as methods 1 and 2.

The in situ X-ray absorption cell used in this study has been described previously [31,32]. Samples were held within a 0.8-mm i.d. quartz capillary with 0.1-mm-thick walls. Gases were metered with electronic mass flow controllers in a manifold capable of producing streams prepared from three different gas sources. H-ZSM-5 was exchanged with MoO<sub>3</sub> with the procedures described above, before X-ray absorption measurements were recorded. Mo<sub>2</sub>O<sub>5</sub><sup>2+</sup>-ZSM-5 was exposed to 90% CH<sub>4</sub>/Ar (Praxair, UHP) at 950 K, and reduction and carburization processes were monitored from X-ray absorption near-edge spectra (XANES) with acquisition method 2; we determined the extent of carburization by monitoring changes in the pre-edge absorption feature. When the pre-edge features became undetectable, samples were exposed to one of two reaction mixtures. Some samples were exposed to pure CH<sub>4</sub> for 1 h, and then extended X-ray absorption fine spectra (EXAFS) were recorded with method 1. The remaining samples were exposed to a reaction mixture with a 0.025 CO<sub>2</sub>/CH<sub>4</sub> molar ratio and the XANES region was monitored with acquisition method 2 until no further spectral changes were detected, at which time a detailed spectrum, including the details of the fine structure, was acquired with method 1.

MoO<sub>3</sub> (Johnson Matthey, 99.5%), MoO<sub>2</sub> (Aldrich, 99.9%),  $\beta$ -Mo<sub>2</sub>C (prepared by temperature-programmed reduction of MoO<sub>3</sub> in 20% H<sub>2</sub>/CH<sub>4</sub> at 973 K [33]), MgMo<sub>2</sub>O<sub>7</sub> (prepared as in [34]), and (NH<sub>4</sub>)<sub>2</sub>Mo<sub>2</sub>O<sub>7</sub> (Strem Chemicals, 99.98%) were diluted with boron nitride and sealed with Kapton tape before we acquired X-ray absorption spectra for these materials with known structures. The  $\beta$ -Mo<sub>2</sub>C sample was passivated before exposure to ambient air; the near-surface regions of the sample contained oxygen. These compounds provide structural and oxidation state standards for the assessment of unknown structures as they evolve during catalysis in various reactant mixtures.

Spectra were analyzed with the use of WinXAS Version 2.1 [35]. Pre-edge and post-edge baselines were subtracted with the use of first- and third-order polynomials, respectively, and the near-edge region was analyzed between 19.90 and 20.12 keV. The absorption background was removed and  $k^2$ -weighted spectra were transformed between 2.6 and 13.0  $\text{\AA}^{-1}$ . The spectra were then corrected for phase shift and fitted in  $R$ -space between 0.5 and 4  $\text{\AA}$  with the use of the Hanning window and FEFFIT [36] to determine interatomic

distances and coordination numbers. Backscattering amplitudes and phase shifts of theoretical standards were generated with the use of FEFF8.0 [37] algorithms, and ATOMS [38] was used to generate the required input files from previously reported atomic coordinates. We determined the amplitude reduction factor,  $S_0^2$ , by fitting experimental Mo foil spectra. Factor analysis was used to identify the principal components in the samples from near-edge spectra recorded during transient experiments. WinXAS software contains a built-in factor analysis code that uses the Malinowski indicator function [39] to estimate the number of pure components, and a target transformation module to identify the pure components [40]. The target transformation algorithm generates an absorption vector of a known reference compound by interpolating its spectra onto the same energy grid as the unknown experimental spectra. A least-squares fitting procedure is then used to determine a transformation vector that will be identical to the absorption vector of the reference compound within experimental error if the reference is indeed a principal component. A goodness-of-fit parameter, or residual, less than 1% is generally considered acceptable [40].

### 3. Results and discussion

#### 3.1. Steady-state catalytic studies

Steady-state catalytic rates and selectivities were first measured on  $\text{Mo}_2\text{O}_5^{2+}$ -ZSM-5 ( $\text{Mo}/\text{Al}_f = 0.41$ ) at 950 K with the use of pure  $\text{CH}_4$  reactants (91 kPa). This catalyst composition led to maximum  $\text{CH}_4$  pyrolysis rates by balancing the number of  $\text{MoC}_x$  species required for  $\text{CH}_4$  activation and the residual Brønsted acid sites required for alkene oligomerization and cyclization, while avoiding dealumination of the zeolite framework via formation of Al molybdate species at higher Mo loadings [17].

Table 1 shows forward rates for product formation at 950 K and 91 kPa  $\text{CH}_4$  after 8.6 and 30.1 ks of contact with reactants. Ethane and ethene  $\eta$  values are almost identical, indicating that their interconversion is equilibrated. The approach to equilibrium for arene synthesis was substantial but decreased with time because of catalyst deactivation by deposition of unreactive residues, which form on active sites within channels, restrict reactant access to such sites, and decrease  $\text{CH}_4$  conversion levels [27]. The sequential nature of arene formation pathways (via  $\text{C}_2$  initial products) led to stronger time-on-stream effects on arene formation rates than on  $\text{C}_2$  formation rates. Thus, the selectivity shifts to primary  $\text{C}_2$  products as deactivation occurs.

$\text{CO}_2$  was added to  $\text{CH}_4$  reactants to probe the effects of  $\text{CO}_2$  concentration on  $\text{CH}_4$  reaction rates and catalyst stability. Steady-state  $\text{CH}_4$  conversion and CO and hydrocarbon yields are shown in Fig. 1 for  $\text{CO}_2/\text{CH}_4$  molar ratios less than 0.1. Samples were first activated by reduction and carburization with pure  $\text{CH}_4$  reactants until hydrocarbon yields

Table 1  
 $\text{CH}_4$  pyrolysis over Mo/H-ZSM-5 (1 g,  $\text{Mo}/\text{Al}_f = 0.41$ , 950 K,  $0.19 \text{ cm}^3 \text{ s}^{-1} \text{ CH}_4$ ; 101.1 kPa,  $\text{CH}_4:\text{Ar} = 9:1$ )

Time on stream (ks)	8.6	30.1
$\text{CH}_4$ conversion (%)	7.0	4.8
Distance to equilibrium ( $\eta$ , %) <sup>a</sup>		
$\text{C}_2\text{H}_4$	87	70
$\text{C}_2\text{H}_6$	86	71
$\text{C}_6\text{H}_6$	54	25
$\text{C}_7\text{H}_8$	57	29
$\text{C}_{10}\text{H}_8$ (naphthalene)	44	19
Forward rates ( $10^{-3} \text{ mol}/(\text{g-atom Mo-s})$ )		
$\text{C}_2$	2.04	1.17
$\text{C}_6\text{H}_6$	2.55	1.16
$\text{C}_7\text{H}_8$	0.14	0.09
$\text{C}_{10}\text{H}_8$	0.47	0.15
Selectivity (% carbon)		
$\text{C}_2\text{H}_4$	3	7
$\text{C}_2\text{H}_6$	2	3
$\text{C}_6\text{H}_6$	54	59
$\text{C}_7\text{H}_8$	3	5
$\text{C}_{10}\text{H}_8$	14	9

<sup>a</sup>  $\eta$ . Distance to equilibrium for each product defined in Eqs. (2)–(5) (Section 2.2).

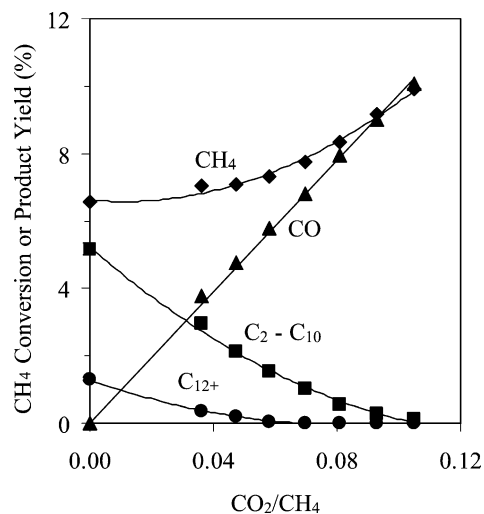


Fig. 1.  $\text{CH}_4$  conversion and hydrocarbon yield as a function of  $\text{CO}_2/\text{CH}_4$  ratio on Mo/H-ZSM-5 (1 g,  $\text{Mo}/\text{Al}_f = 0.41$ , 950 K,  $0.19 \text{ cm}^3 \text{ s}^{-1} \text{ CH}_4$ , 91 kPa  $\text{CH}_4$ ).

reached maximum values ( $\sim 2$  h);  $\text{CO}_2$  was then added.  $\text{CH}_4$  conversion remained constant at  $\sim 7\%$  for  $\text{CO}_2/\text{CH}_4$  ratios below 0.064;  $\text{CO}_2$  was not detected in the effluent with these reactant mixtures. At slightly higher  $\text{CO}_2/\text{CH}_4$  ratios,  $\text{CH}_4$  conversion increased proportionally with  $\text{CO}_2$  concentration. Methane conversions were very similar to the sum of hydrocarbons and CO (from  $\text{CH}_4$ , defined in the Experimental section) yields; no detectable  $\text{C}_{12+}$  products were formed at these moderate  $\text{CO}_2$  concentrations. Fig. 2 shows  $\text{CH}_4$  conversion and hydrocarbon and CO yields for reactant mixtures with  $\text{CO}_2/\text{CH}_4$  ratios of 0, 0.05, and 0.1 after activation in pure  $\text{CH}_4$  for 2 h. Hydrocarbon yields were 2.1% at a 0.05  $\text{CO}_2/\text{CH}_4$  ratio and did not decrease even



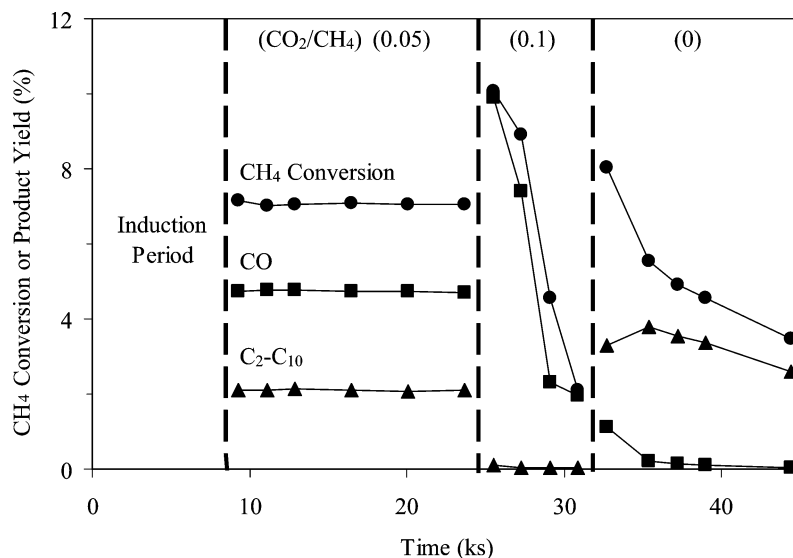


Fig. 2. CH<sub>4</sub> conversion and hydrocarbon yield as a function of time on Mo/H-ZSM-5 (1 g, Mo/Al<sub>f</sub> = 0.41, 950 K, 0.19 cm<sup>3</sup> s<sup>-1</sup> CH<sub>4</sub>, 91 kPa CH<sub>4</sub>).

after 15 ks; only traces of C<sub>12+</sub> hydrocarbons were formed. At a CO<sub>2</sub>/CH<sub>4</sub> ratio of 0.1, the initial CH<sub>4</sub> conversion was ~10%, CO<sub>2</sub> was completely consumed within the catalyst bed, and hydrocarbons were virtually undetected at less than two orders of magnitude of their yields in CO<sub>2</sub> free feeds (Fig. 2, right panel). With this reactant mixture, CH<sub>4</sub> conversion decreased abruptly to undetectable levels after ~1 h. Removal of CO<sub>2</sub> from the reactant stream led to the recovery of catalytic rates, after an activation period of 3 ks, during which CO was formed and hydrocarbons increased to maximum rates (Fig. 2, right panel).

The lower hydrocarbon yields obtained with CO<sub>2</sub> coreactants may reflect thermodynamic or kinetic effects. H<sub>2</sub> formed via CH<sub>4</sub>-CO<sub>2</sub> reforming would decrease equilibrium CH<sub>4</sub> conversion levels and increase rates for the reverse of the dehydrogenation steps required to form alkenes and arenes. Adsorbed organic species may be removed continuously by CO<sub>2</sub>, thus inhibiting chain growth processes requiring C-C bond formation, but ultimately replacing carbidic carbon in MoC<sub>x</sub> with O-atoms until CO<sub>2</sub> is depleted along the catalyst bed. CO products of CH<sub>4</sub>-CO<sub>2</sub> mixtures may also form unreactive carbon species via Boudouard reactions that impede access to active sites. We consider each of these possible effects below.

Net rates were corrected for approach to equilibrium to assess the role of H<sub>2</sub> formed in CH<sub>4</sub>-CO<sub>2</sub> reactions on pyrolysis forward rates. The resulting (forward) arene synthesis rates decreased with increasing CO<sub>2</sub> concentration (Fig. 3). Equilibrium calculations for combined pyrolysis and CO<sub>2</sub> reforming reactions, made with thermodynamic data [41,42], showed that net hydrocarbon yields decreased with increasing CO<sub>2</sub> feed concentration because of the H<sub>2</sub> formed in CO<sub>2</sub> reforming reactions. If H<sub>2</sub> were solely responsible, however, for the observed effects of CO<sub>2</sub> on hydrocarbon synthesis rates, forward arene synthesis rates

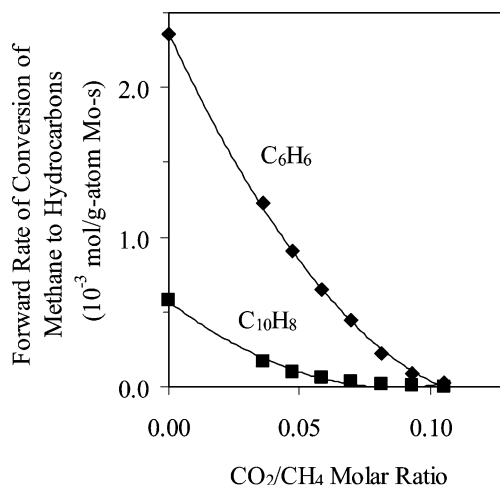


Fig. 3. Forward product synthesis rates as a function of CO<sub>2</sub>/CH<sub>4</sub> ratio on Mo/H-ZSM-5 (1 g, Mo/Al<sub>f</sub> = 0.41, 950 K, 0.19 cm<sup>3</sup> s<sup>-1</sup> CH<sub>4</sub>, 91 kPa CH<sub>4</sub>).

would be independent of CO<sub>2</sub> concentration, in contradiction to the data shown in Fig. 3.

We next consider the effect of H<sub>2</sub> on pyrolysis rates independently of CO<sub>2</sub> with H<sub>2</sub>/CH<sub>4</sub> reactants. H<sub>2</sub> can decrease net arene synthesis rates because of thermodynamic effects, which are accounted for through our use of forward rates, or via scavenging of reactive carbon and suppression of C-C bond formation pathways. Fig. 4a shows benzene forward rates as a function of average H<sub>2</sub> pressure (defined as the mean of its inlet and outlet values) with both H<sub>2</sub>/CH<sub>4</sub> and CO<sub>2</sub>/CH<sub>4</sub> reactants (at 950 K and 91 kPa CH<sub>4</sub>). We calculated inlet H<sub>2</sub> pressures for CO<sub>2</sub>/CH<sub>4</sub> mixtures by assuming that CO<sub>2</sub> is depleted near the bed inlet and H<sub>2</sub> forms with the stoichiometry of CH<sub>4</sub>-CO<sub>2</sub> reactions. Forward rates of benzene synthesis decreased with increasing H<sub>2</sub> pressure in H<sub>2</sub>/CH<sub>4</sub> feeds, indicating that H<sub>2</sub> kinetically inhibits CH<sub>4</sub>

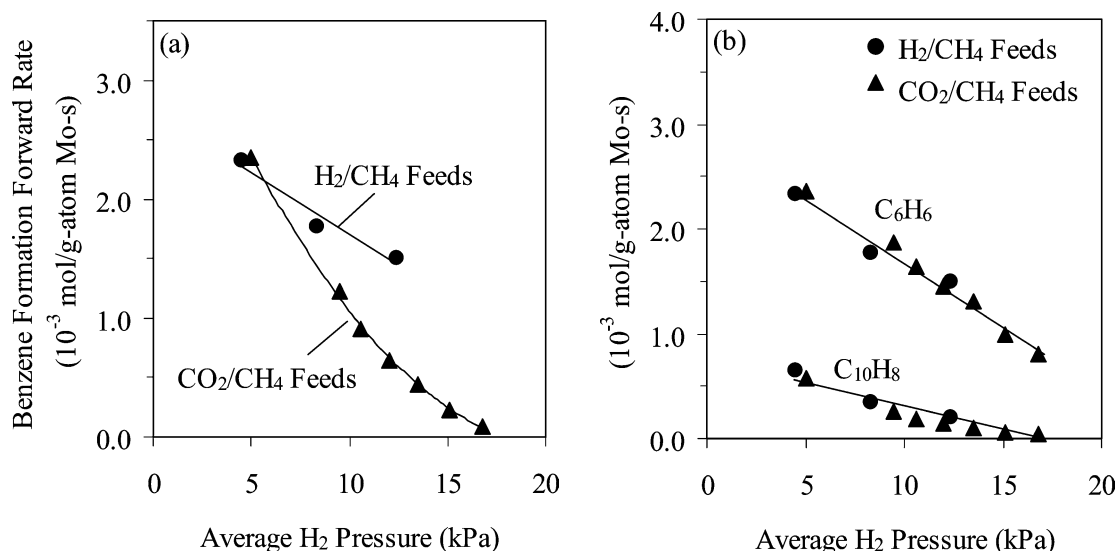


Fig. 4. Forward benzene formation rate as a function of average H<sub>2</sub> pressure on Mo/H-ZSM-5 (1 g, Mo/Al<sub>f</sub> = 0.41, 950 K, 0.19 cm<sup>3</sup> s<sup>-1</sup> CH<sub>4</sub>, 91 kPa CH<sub>4</sub>) assuming (a) CO<sub>2</sub> is completely consumed near bed inlet and (b) CO<sub>2</sub> is consumed at an intermediate point along the bed proportional to the CO<sub>2</sub> inlet concentration given by Eqs. (6) and (7). The average H<sub>2</sub> pressure is defined as the arithmetic mean of the inlet and outlet H<sub>2</sub> partial pressures. The inlet H<sub>2</sub> partial pressure for CO<sub>2</sub>/CH<sub>4</sub> mixtures is defined as the partial pressure of H<sub>2</sub> produced in CO<sub>2</sub> reforming reactions.

pyrolysis reactions, because we take thermodynamic effects into account by using Eqs. (2)–(5) to calculate forward rates. Benzene synthesis forward rates were always higher with H<sub>2</sub>/CH<sub>4</sub> than with CO<sub>2</sub>/CH<sub>4</sub> reactants for any given average H<sub>2</sub> pressure. Therefore, the lower benzene forward rates observed with CO<sub>2</sub>/CH<sub>4</sub> mixtures are not caused only by inhibition by the H<sub>2</sub> formed (in CH<sub>4</sub>–CO<sub>2</sub> reforming reactions) near the bed inlet.

The data in Fig. 2 show that at CO<sub>2</sub> conversions below 100%, hydrocarbon yields decrease by two orders of magnitude compared with those with CO<sub>2</sub>-free feeds. CO<sub>2</sub> scavenges C\* before C–C bond formation can occur, thus preventing pyrolysis reactions at any reactor position that contains unreacted CO<sub>2</sub>. Thus, the fraction of the catalyst bed that remains available for CH<sub>4</sub> pyrolysis reactions decreases with increasing CO<sub>2</sub> concentration. CO<sub>2</sub> reforming rates on Ni and noble metal catalysts have been shown to be independent of CO<sub>2</sub> and proportional to CH<sub>4</sub> concentrations [43,44]; therefore, the fraction of the catalyst exposed to CO<sub>2</sub> should be proportional to the inlet CO<sub>2</sub> concentration at these low CO<sub>2</sub>/CH<sub>4</sub> ratios. Forward pyrolysis rates (Fig. 4a) thus reflect only that part of the bed remaining after CO<sub>2</sub> depletion. We account for this smaller amount of active catalyst by using the CO<sub>2</sub> concentration where no hydrocarbons are detected as the threshold CO<sub>2</sub> concentration, C<sub>max</sub>, and assuming that for feeds with CO<sub>2</sub> inlet concentration, C<sub>i</sub>, the CO<sub>2</sub> is completely consumed at a bed length, L<sub>i</sub>, equal to

$$L_i = (LC_i)/C_{\max}, \quad (6)$$

where *L* is the length of the fixed-bed reactor. Forward rates corrected for effective bed length are then equal to

$$r_{\text{forward,eff}} = \frac{r_{\text{forward}}}{1 - L_i/L}. \quad (7)$$

The *r*<sub>forward,eff</sub> vs average H<sub>2</sub> partial pressure is plotted in Fig. 4b. Benzene forward rates for H<sub>2</sub>/CH<sub>4</sub> and CO<sub>2</sub>/CH<sub>4</sub> feeds collapse onto a single line, confirming our new model for the complete suppression of pyrolysis reactions by CO<sub>2</sub>. Naphthalene synthesis rates for CO<sub>2</sub>/CH<sub>4</sub> and H<sub>2</sub>/CH<sub>4</sub> feeds also lie along the same line.

The effective forward rates in Fig. 4 suggest that the lower pyrolysis yields with CO<sub>2</sub>/CH<sub>4</sub> mixtures occur as a result of a shorter active catalyst bed available for pyrolysis as a result of CO<sub>2</sub> scavenging of active C\* near the bed inlet. Yet we observe, as have others [24], that pyrolysis rates are much more stable with time on stream when CO<sub>2</sub> is present in CH<sub>4</sub> feeds, even though pyrolysis occurs only in those regions of the bed where CO<sub>2</sub> is no longer present. Such regions of the bed can detect the presence of CO<sub>2</sub> in the inlet stream only through the presence of the H<sub>2</sub> and CO products formed in CH<sub>4</sub>–CO<sub>2</sub> reactions. First-order deactivation constants for hydrocarbon synthesis were 0.011 and 0.0008 ks<sup>-1</sup>, with CH<sub>4</sub> (5 kPa average H<sub>2</sub> pressure ⟨H<sub>2</sub>⟩) and 0.06 CO<sub>2</sub>/CH<sub>4</sub> (12.5 kPa ⟨H<sub>2</sub>⟩) feeds, respectively, as shown in Table 2. For a H<sub>2</sub>/CH<sub>4</sub> feed with an average H<sub>2</sub> pressure (12 kPa ⟨H<sub>2</sub>⟩) similar to that prevalent after CO<sub>2</sub> depletion with 0.06 CO<sub>2</sub>/CH<sub>4</sub> reactants, the deactivation constant was 0.001 ks<sup>-1</sup>, a value very similar to that obtained with CO<sub>2</sub> coreactants (0.0008 ks<sup>-1</sup>). The similar deactivation constants for feeds with similar average H<sub>2</sub> pressures (12–12.5 kPa) but different inlet compositions confirm that the sole effect of CO<sub>2</sub> coreactants on deactivation is to form H<sub>2</sub>, which acts as the deactivation inhibitor in downstream pyrolysis reactions of the catalyst bed, within which CO<sub>2</sub> could not have any more direct effects because it is no longer available. This exclusive role of H<sub>2</sub> in inhibiting deactivation processes contrasts with previous claims attributing it

Table 2

First order deactivation constants and benzene forward rates over Mo-ZSM-5 (1 g, Mo/Al<sub>f</sub> = 0.41, 950 K, 0.19 cm<sup>3</sup> s<sup>-1</sup> CH<sub>4</sub>, 91 kPa CH<sub>4</sub>) with different average H<sub>2</sub> partial pressures

Average H <sub>2</sub> pressure of feed mixture (kPa)	$k_d$ (10 <sup>-2</sup> ks <sup>-1</sup> )			Benzene rate (10 <sup>-3</sup> mol/(g-atom Mo-s))		
	CH <sub>4</sub>	H <sub>2</sub> /CH <sub>4</sub>	CO <sub>2</sub> /CH <sub>4</sub>	CH <sub>4</sub>	H <sub>2</sub> /CH <sub>4</sub>	CO <sub>2</sub> /CH <sub>4</sub> <sup>a</sup>
5	1.10	–	–	2.35	–	–
12	–	0.10	–	–	1.50	–
12.5	–	–	0.08	–	–	1.45

<sup>a</sup> Benzene forward rate corrected for effective bed used for pyrolysis (Eqs. (6) and (7)).

directly to CO<sub>2</sub> scavenging of C\* via reverse Boudouard reactions [24].

Forward rates measured as a function of inlet composition indicate that the catalyst bed can be described as two discrete sections, catalyzing reforming and pyrolysis reactions, at low CO<sub>2</sub>/CH<sub>4</sub> ratios. Pyrolysis does not occur while CO<sub>2</sub> is available because it effectively scavenges C\* intermediates required for chain growth. The downstream pyrolysis section acts as a catalyst bed with an inlet stream containing CH<sub>4</sub> and equimolar amounts of H<sub>2</sub> and CO. The shorter effective bed for pyrolysis and the thermodynamic effects of H<sub>2</sub> formed in the reforming section lead to lower hydrocarbon yields than with pure CH<sub>4</sub> inlet streams, but also to lower deactivation rates as a result of the role of H<sub>2</sub> in preventing the formation of unreactive residues, probably large polynuclear aromatics requiring sequential dehydrogenation steps reversed by H<sub>2</sub>.

The active Mo phase within pyrolysis sections of the bed consists of small carbide clusters similar to Mo<sub>2</sub>C [16,45], but the structure and oxidation state of the section of the bed exposed to CO<sub>2</sub> remain unclear. In the sections that follow, we explore the structural and catalytic consequences of CO<sub>2</sub>/CH<sub>4</sub> mixtures by mass spectrometric analysis of the bed effluent during compositional transients and in situ X-ray absorption spectroscopy to provide evidence that oxidation of Mo carbides at high CO<sub>2</sub> concentrations forms a Mo phase that is inactive for C–H bond breaking and therefore for catalytic pyrolysis of CH<sub>4</sub>.

### 3.2. Transient evolution of products during contact with CO<sub>2</sub>/CH<sub>4</sub> reactant mixtures

The removal of C\* by CO<sub>2</sub> to form CO and the potential replacement of the C\* species in MoC<sub>x</sub> by oxygen to form MoO<sub>x</sub> species inactive in pyrolysis and even reforming reactions may account for the deactivation of Mo-ZSM-5 observed at high CO<sub>2</sub> concentrations (Fig. 2). The resulting depletion of reactive C\* (or CH<sub>x</sub>\*) monomers would prevent C–C bond formation within regions in the reactor containing CO<sub>2</sub>. We examined these effects by measuring changes in effluent composition, as inlet CO<sub>2</sub> concentrations were abruptly changed in an effort to measure the number of O atoms added to or removed from working catalysts in environments containing different CO<sub>2</sub> concentrations.

Fig. 5a shows the CO, H<sub>2</sub>O, H<sub>2</sub>, C<sub>2</sub>H<sub>4</sub>, and C<sub>6</sub>H<sub>6</sub> formation rates and CH<sub>4</sub> conversion during initial contact of

Mo<sub>2</sub>O<sub>5</sub><sup>2+</sup>-ZSM-5 with CH<sub>4</sub> at 950 K. H<sub>2</sub>, H<sub>2</sub>O, and CO were initially detected as a result of the reduction and carburization of trace amounts of unexchanged MoO<sub>3</sub> [29]; these products inhibit the reduction and carburization of less reducible exchanged Mo-oxo dimers. As these dimers ultimately converted to MoC<sub>x</sub> clusters, H<sub>2</sub>O concentrations decreased and H<sub>2</sub> and CO formation rates increased sharply until all of the O atoms in Mo<sub>2</sub>O<sub>5</sub><sup>2+</sup> were removed and catalysts reached maximum CH<sub>4</sub> pyrolysis rates. Initial exposure of Mo<sub>2</sub>O<sub>5</sub><sup>2+</sup>-ZSM-5 to CH<sub>4</sub> (CO<sub>2</sub>/CH<sub>4</sub> = 0; Fig. 5a) removed 2.5 ± 0.05 O atoms per Mo atom (Fig. 6, left panel), measured from the concentration of oxygen-containing products (CO, CO<sub>2</sub> (x2), H<sub>2</sub>O), indicating that all nonzeolitic O atoms in exchanged Mo<sub>2</sub>O<sub>5</sub><sup>2+</sup> were removed, as shown previously [18]. Benzene, a representative pyrolysis product, was first detected at ~ 500 s (Fig. 5a) and reached maximum synthesis rates (5 × 10<sup>-4</sup> mol/(g-atom Mo-s)) before decreasing gradually as deactivation occurred.

Next we consider the transient behavior of Mo<sub>2</sub>O<sub>5</sub><sup>2+</sup>-ZSM-5 samples first carburized in pure CH<sub>4</sub> (for 1 h) and then exposed to reactants with a CO<sub>2</sub>/CH<sub>4</sub> molar ratio of 0.022 (Fig. 5b). During initial carburization and catalytic CH<sub>4</sub> pyrolysis, CH<sub>4</sub> conversion decreased to ~ 1% after 1 h before CO<sub>2</sub> was introduced into the pure CH<sub>4</sub> stream. CO<sub>2</sub> was completely converted and CH<sub>4</sub> conversion increased immediately to ~ 3% upon the introduction of CO<sub>2</sub>. The CH<sub>4</sub> conversion oscillations in Fig. 5b reflect pumping fluctuations in the mass spectrometer; they occurred in this experiment also before CO<sub>2</sub> addition and do not reflect oscillations in catalytic rates. Measured net benzene synthesis rates decreased from 2 × 10<sup>-4</sup> to 5 × 10<sup>-5</sup> mol/(g-atom Mo-s) during CO<sub>2</sub> addition.

We measured the amount of oxygen introduced into this sample during contact with this CO<sub>2</sub>-containing reactant mixture by subtracting the CO formed from the amount of CO required for CO<sub>2</sub> reforming of CH<sub>4</sub>. H<sub>2</sub>O, which forms in concurrent water–gas-shift reactions, was below the detection limit, as expected from water–gas shift equilibrium calculations under these reaction conditions (~ 10<sup>-9</sup> kPa). CO<sub>2</sub>/CH<sub>4</sub> inlet ratios of 0.022 and 0.055 led to the introduction of 0.28 ± 0.01 and 1.8 ± 0.03 O atoms per Mo atom (Fig. 6, middle panel), respectively, into MoC<sub>x</sub> clusters formed during initial contact with pure CH<sub>4</sub> reactants. This suggests that some C\* in MoC<sub>x</sub> is replaced with O\* at the beginning of the bed where CO<sub>2</sub> was present, but the catalyst bed remains active for CO<sub>2</sub> reforming and CH<sub>4</sub> pyrolysis

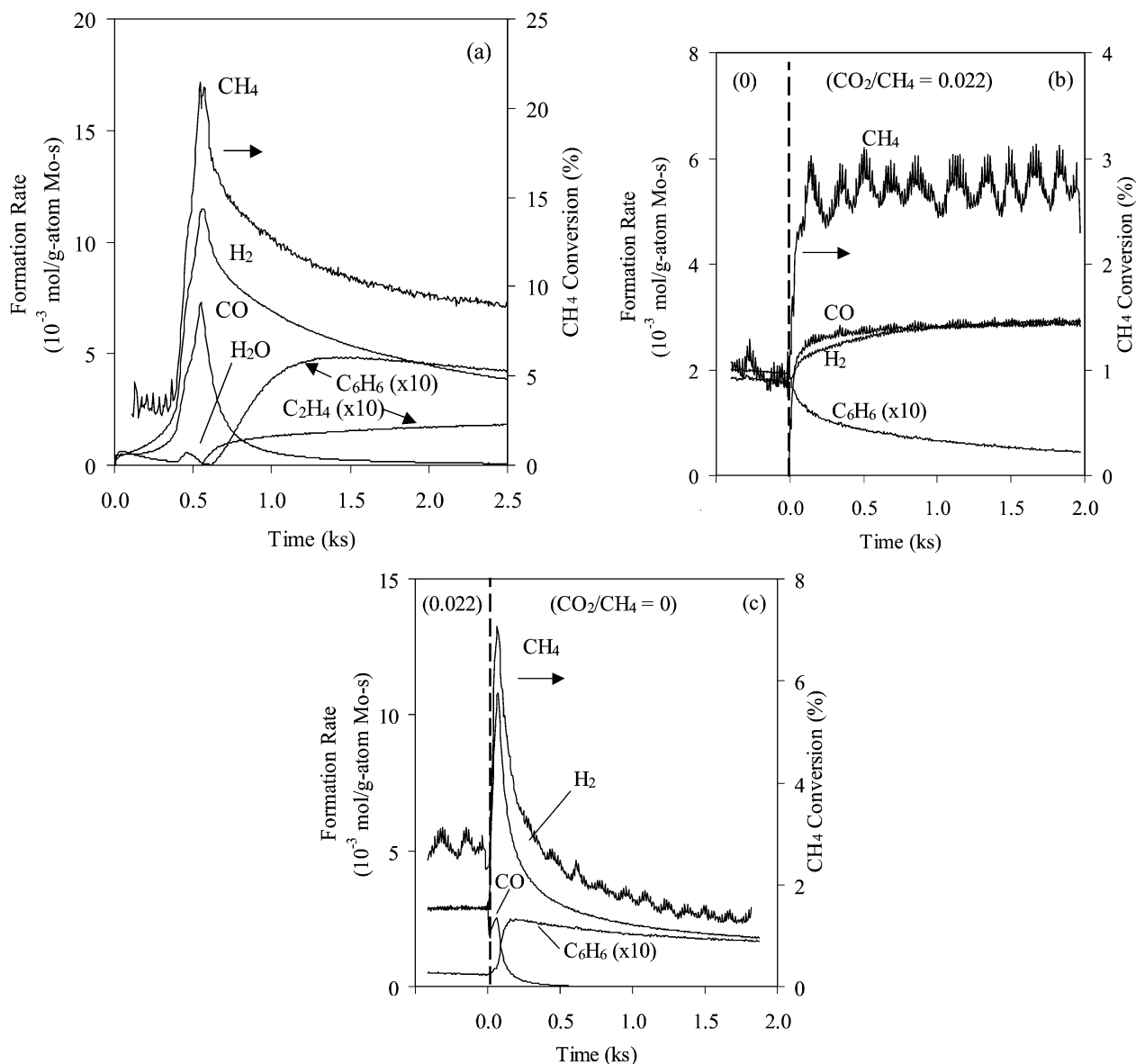


Fig. 5. Transient product formation rates and CH<sub>4</sub> conversion during reactions of CO<sub>2</sub>/CH<sub>4</sub> mixtures on Mo/H-ZSM-5 (1 g, Mo/Al<sub>f</sub> = 0.41, 950 K, 1 cm<sup>3</sup> s<sup>-1</sup>, 54 kPa CH<sub>4</sub>) (a) CO<sub>2</sub>/CH<sub>4</sub> = 0, (b) 0.022 CO<sub>2</sub>/CH<sub>4</sub>, and (c) CO<sub>2</sub>/CH<sub>4</sub> = 0 after (b).

at these CO<sub>2</sub> concentrations. Fig. 5c shows product evolution profiles after a 0.022 CO<sub>2</sub>/CH<sub>4</sub> stream was replaced with pure CH<sub>4</sub> reactants. CH<sub>4</sub> conversion increased sharply to 7%, and then benzene synthesis rates gradually returned to the values measured during initial contact with pure CH<sub>4</sub> reactants ( $\sim 2 \times 10^{-4}$  mol/(g-atom Mo-s)) in  $\sim 1$  ks. The number of O atoms removed during exposure to pure CH<sub>4</sub> reactants was measured from the number of CO molecules formed during contact with pure CH<sub>4</sub> reactants (only traces of H<sub>2</sub>O and CO<sub>2</sub> formed) (Fig. 6, right panel). This procedure yielded  $0.31 \pm 0.01$  and  $1.7 \pm 0.03$  O atoms removed per Mo atom for CO<sub>2</sub>/CH<sub>4</sub> ratios of 0.022 and 0.055, respectively (Table 3). These values are consistent with the amounts of oxygen deposited on active oxygen-free MoC<sub>x</sub> structures during contact with each of these CO<sub>2</sub>-containing streams (0.28 and 1.8 O/Mo, respectively).

After CO<sub>2</sub> was removed from the inlet stream, benzene synthesis rates returned to values measured before CO<sub>2</sub> introduction, but not to those measured after initial activation of fresh exchanged samples in pure CH<sub>4</sub> streams. The formation of carbon deposits on acid sites and external surfaces has been examined by X-ray photoelectron spectroscopy and reactivity studies [27,46]; unreactive carbon residues restrict channel entrances, and their formation is essentially irreversible, except by treatment in O<sub>2</sub> at high temperatures [17]. Oxidation of MoC<sub>x</sub>-ZSM-5 in O<sub>2</sub> at 973 K restores more than 90% of initial pyrolysis rates [17] by converting deactivated MoC<sub>x</sub> clusters to MoO<sub>3</sub> and redispersing it as Mo<sub>2</sub>O<sub>5</sub><sup>2+</sup> dimers above 623 K. In contrast, MoC<sub>x</sub> oxidation in CO<sub>2</sub>/CH<sub>4</sub> reactant mixtures does not remove unreactive carbon deposits formed during pyrolysis at other locations, even though these mixtures led to significant conversion of



Table 3

O-atom addition/removal from  $\text{Mo}_2\text{O}_5^{2+}$ -ZSM-5 (1 g,  $\text{Mo}/\text{Al}_f = 0.41$ , 950 K,  $1 \text{ cm}^3 \text{ s}^{-1}$ , 54 kPa  $\text{CH}_4$ , 6 kPa Ar, balance He with 101.3 kPa total)

$\text{CO}_2/\text{CH}_4$	(O-atoms) removed/Mo		
	During initial contact $\text{Mo}_2\text{O}_5^{2+}$ with $\text{CH}_4$	After carburization and introduction of $\text{CO}_2/\text{CH}_4$	After reintroduction of $\text{CH}_4$
0.022	+2.6	-0.28	+0.31
0.055	+2.5	-1.8	+1.7

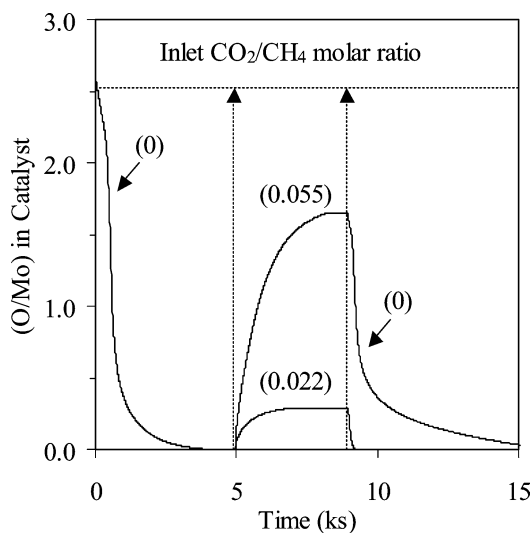


Fig. 6. (O/Mo) in catalyst as a function of time on Mo/H-ZSM-5 (1 g,  $\text{Mo}/\text{Al}_f = 0.41$ , 950 K,  $1 \text{ cm}^3 \text{ s}^{-1}$ , 54 kPa  $\text{CH}_4$ ). Numbers in parenthesis denote  $\text{CO}_2/\text{CH}_4$  ratio in feed.

$\text{MoC}_x$  species to the corresponding suboxides. The formation of these unreactive deposits appears to be inhibited in  $\text{CO}_2$ -containing feeds, as shown by the low deactivation rates observed for reactant mixtures with  $\text{CO}_2/\text{CH}_4$  ratios below 0.1, which reflect the presence of  $\text{H}_2$  formed via  $\text{CO}_2$  reforming near the bed inlet.  $\text{CO}_2$  addition did lead to the ultimate replacement of chemisorbed carbon with oxygen as illustrated in Fig. 7. Fig. 7 depicts a  $\text{Mo}_2\text{C}$  particle formed during activation processes in  $\text{CH}_4$  described above and suddenly exposed to a  $\text{CO}_2/\text{CH}_4$  reactant mixture.  $\text{CO}_2$  can react directly with a vacancy to form CO and  $\text{O}^*$ , or it can react

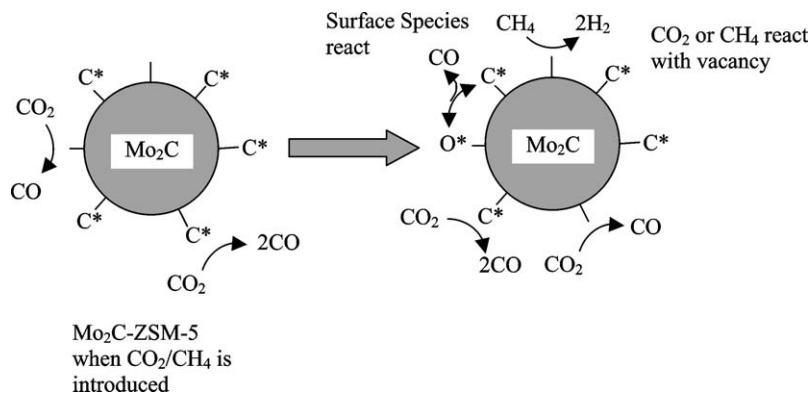


Fig. 7. Schematic representation of  $\text{MoC}_x$ -ZSM-5 surface in  $\text{CO}_2/\text{CH}_4$  ( $\ll 1$ ) reactant mixtures. The left cluster depicts initial exposure of  $\text{Mo}_2\text{C}$  to  $\text{CO}_2/\text{CH}_4$ , and the right cluster depicts reactions involving surface species and gaseous  $\text{CH}_4$  and  $\text{CO}_2$ .

with a surface  $\text{C}^*$  to form two CO molecules and a vacancy (as in Eq. (1)). Similar oxidative deactivation pathways on bulk and supported  $\text{Mo}_2\text{C}$  and WC during  $\text{CO}_2$  reforming of  $\text{CH}_4$  were proposed by Green et al. [28]. O atoms, generated by dissociation of  $\text{CO}_2$ , react with carbon in carbide structures to form a carbon vacancy that can then be filled with additional O atoms from  $\text{CO}_2$ , leading to the ultimate oxidation of  $\text{MoC}_x$  structures. Such vacancies can react also with  $\text{C}^*$  formed via  $\text{CH}_4$  dissociation to reform a stoichiometric carbide; these processes are in a state of dynamic balance during steady catalysis, as depicted in Fig. 7.

These conclusions about reduction–carburization–oxidation cycles are based on rigorous chemical balancing of inlet and outlet streams; they do not, however, provide direct evidence for structural changes in Mo centers during contact with reactant streams with different  $\text{CO}_2/\text{CH}_4$  ratios. In the following section, we describe catalyst structure and electronic properties with the use of near-edge (XANES) and extended fine structure (EXAFS) analysis of X-ray absorption spectra during catalytic reactions of  $\text{CH}_4$ – $\text{CO}_2$  mixtures.

### 3.3. In situ near-edge and fine structure X-ray absorption spectra at the Mo K-edge

Near-edge X-ray absorption spectra are shown in Fig. 8 for exchanged  $\text{Mo}_2\text{O}_5^{2+}$ -ZSM-5 prepared from  $\text{Mo}_3/\text{H-ZSM-5}$  physical mixtures and for reference Mo compounds with known structure. The spectra for the initial physical mixtures resembled that for crystalline  $\text{MoO}_3$ , within which Mo atoms reside in distorted octahedral coordination. Thermal treatment to 950 K in 20%  $\text{O}_2/\text{He}$  led to gradual changes in the near-edge spectra of these mixtures. The spectra ul-

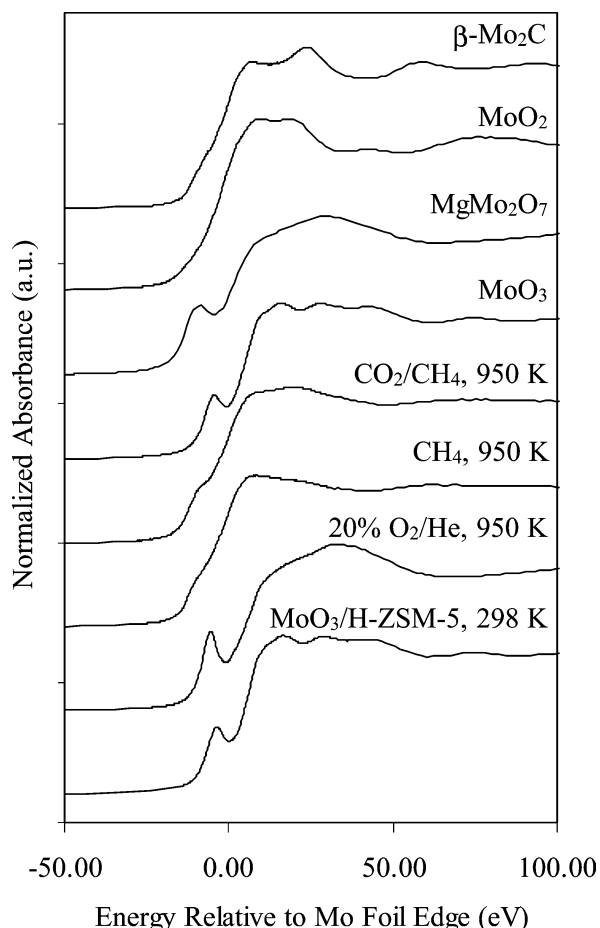


Fig. 8. Mo  $K$ -edge near-edge spectra for  $\beta$ - $\text{Mo}_2\text{C}$  exposed to air,  $\text{MoO}_2$ ,  $\text{MgMo}_2\text{O}_7$ ,  $\text{MoO}_3$  and physical mixtures of  $\text{MoO}_3/\text{H-ZSM-5}$  ( $\text{Mo}/\text{Al}_f = 0.41$ ) during treatment in 20%  $\text{O}_2/\text{He}$  at 298 and 950 K,  $\text{CH}_4$  at 950 K and  $\text{CO}_2/\text{CH}_4 = 0.025$  at 950 K.

Table 4

Edge energy position of Mo (relative to Mo foil edge at 20,000 eV) in reference compounds and  $\text{Mo}/\text{H-ZSM-5}$

Compound	$\Delta E_0$ (eV)
$\text{MoO}_3$	4.8
$\beta$ - $\text{Mo}_2\text{C}$	0.2
$(\text{NH}_4)_2\text{Mo}_2\text{O}_7$	4.4
$\text{MoO}_3/\text{H-ZSM-5}$	4.3
$\text{Mo}_2\text{O}_5^{2+}$ -ZSM-5	4.9
$\text{Mo}_2\text{O}_5^{2+}$ -ZSM-5 after treatment in $\text{CH}_4$ at 950 K for 1 h	0.2
$\text{Mo}_2\text{O}_5^{2+}$ -ZSM-5 after treatment in $\text{CH}_4$ at 950 K for 1 h then in $\text{CO}_2/\text{CH}_4 = 0.025$ at 950 K for 1 h	1.9

timately resemble that for  $\text{MgMo}_2\text{O}_7$ , which contains ditetrahedral Mo centers, indicating the presence of  $\text{Mo}_2\text{O}_5^{2+}$ -ZSM-5 structures anchored at vicinal exchange sites [19].  $\text{Mo}_2\text{O}_5^{2+}$ -ZSM-5 exhibits a pre-edge feature, which arises from  $1s \rightarrow 4d$  electronic transitions; these transitions are dipole-forbidden for centrosymmetric Mo centers. As electrons are placed in  $4d$  orbitals during reduction of  $\text{Mo}^{6+}$  cations, these transitions become less probable and pre-edge features become weaker and ultimately undetectable in  $\text{Mo}^0$

[19,47,48].  $\text{MoO}_2$  contains partially filled  $4d$  shells and does not show a pre-edge feature.  $\text{Mo}_2\text{O}_5^{2+}$ -ZSM-5 has a more intense pre-edge feature (Fig. 8) than  $\text{MoO}_3$ , indicating a change in Mo coordination from distorted octahedral to tetrahedral during thermal treatments leading to exchange [49,50]. Pre-edge features in  $\text{Mo}_2\text{O}_5^{2+}$ -ZSM-5 disappeared upon contact with  $\text{CH}_4$  at 950 K for 1 h, indicating that Mo-oxo species reduced and carburized during catalysis. Subsequent exposure of  $\text{MoC}_x$  structures to reactants with  $\text{CO}_2/\text{CH}_4$  ratios of 0.025 for 1 h led to the reappearance of pre-edge features, albeit with much lower intensity than in fresh exchanged  $\text{Mo}_2\text{O}_5^{2+}$ -ZSM-5.

Changes in the absorption edge energy were also detected during catalytic reactions with other  $\text{CO}_2/\text{CH}_4$  reactant mixtures (Table 4). The edge energy was taken as the first inflection point in the absorption edge (or the first inflection after the pre-edge feature, if present). Fresh exchanged  $\text{Mo}_2\text{O}_5^{2+}$ -ZSM-5 showed an edge energy (relative to  $\text{Mo}^0$ ) at 4.90 eV, similar to that of  $\text{MoO}_3$  (4.8 eV) and corresponding to that of  $\text{Mo}^{6+}$ . After exposure to  $\text{CH}_4$ , the edge shifts to 0.2 eV and then back to 1.9 eV after contact with a 0.025  $\text{CO}_2/\text{CH}_4$  mixture at 950 K for 1 h. These data show that reduction and carburization occur during activation in pure  $\text{CH}_4$  and that these processes are reversed, to some extent, as  $\text{CO}_2$  is introduced along with  $\text{CH}_4$  reactants. As  $\text{CO}_2$  is depleted along the plug-flow reactor cell, the composition of the gas phase changes, leading to a mixture of Mo structures and oxidation states, all of which are sampled by the X-ray beam during these absorption measurements.

Factor analysis was used to identify principal components from near-edge spectra. This method has been used previously to identify pure components contributing to X-ray absorption spectra [40,49,51,52]. First, factor analysis was used to determine that two principal components contributed to the 11 near-edge spectra acquired during transient  $\text{CO}_2/\text{CH}_4 = 0.025$  addition. The identities of pure components in  $\text{CO}_2/\text{CH}_4$  feed transients were established with the use of a target transformation algorithm in WinXAS 2.1 (see details in the Experimental section).  $\text{Mo}_2\text{O}_5^{2+}$ -ZSM-5 treated in  $\text{CH}_4$  for 1–6 h in  $\text{CH}_4$  at 950 K was shown to exist as 0.5–0.6 nm  $\text{Mo}_2\text{C}$  clusters from multiple-scattering simulations of the absorption fine structure [19,45].  $\text{MoC}_x$  was identified as a principal component with a residual of 0.26% in carburized Mo-ZSM-5 in this study; residuals lower than 1% indicate an unequivocal identification of a principal component [40]. The fresh exchanged  $\text{Mo}_2\text{O}_5^{2+}$ -ZSM-5 sample gave a residual of 5%, a relatively poor fit compared with the carburized Mo-ZSM-5 structural standard. Bulk  $\text{MoO}_3$  gave a residual of 2.6%, considerably better than  $\text{Mo}_2\text{O}_5^{2+}$ -ZSM-5, but still high. Oxycarbides, as depicted in Fig. 7, are most likely the dominant species at 0.025  $\text{CO}_2/\text{CH}_4$ , and therefore neither one of the reference compounds accurately describes the experimental transient spectra. In lieu of suitable standards, the oxidation of active Mo carbides by  $\text{CO}_2/\text{CH}_4$  mixtures can be described by two principal com-

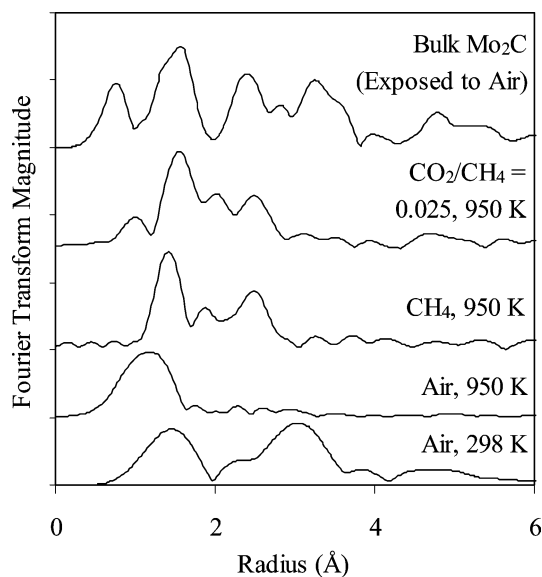


Fig. 9. Radial structure function (RSF) for  $\beta$ -Mo<sub>2</sub>C exposed to air and for MoO<sub>3</sub>/H-ZSM-5 (Mo/Al<sub>F</sub> = 0.41) during treatment in 20% O<sub>2</sub>/He at 298 and 950 K, CH<sub>4</sub> at 950 K and CO<sub>2</sub>/CH<sub>4</sub> = 0.025 at 950 K. RSF for each sample was generated by Fourier-transform magnitude of  $k^2$ -weighted EXAFS.

ponents, one of which is Mo<sub>2</sub>C, but the identification of the other principal components remains ambiguous at this time.

A Fourier transform of the fine structure region gives a radial structure function around Mo absorbers (e.g., Fig. 9 for Mo<sub>2</sub>O<sub>5</sub><sup>2+</sup>-ZSM-5). The intensity of the features is related to the number of scatterers at a given distance from Mo atoms, which is corrected in structural fits by thermal and static disorder and by the scattering cross section of the neighboring atoms. Fig. 10 shows experimental and fitted  $k^2$ -weighted EXAFS and radial scattering functions for Mo<sub>2</sub>O<sub>5</sub><sup>2+</sup>-ZSM-5; the parameters arising from structural refinement procedures are shown in Table 5. These fine structure spectra for exchanged Mo<sub>2</sub>O<sub>5</sub><sup>2+</sup>-ZSM-5 in 20% O<sub>2</sub>/He were described via multiple scattering simulations with MgMo<sub>2</sub>O<sub>7</sub> standards as the starting point. The resulting simulated structures confirmed that each Mo atom has four oxygen neighbors in a tetrahedral arrangement at a distance of 0.16–0.18 nm. Scattering from next-nearest neighboring Mo or Al was not detected in the experiments or in simulated radial structure functions because of a  $\pi$  phase shift in multiple scattering paths, which leads to destructive interference of scattered electrons [19].

Several features emerged in the radial structure function of Mo<sub>2</sub>O<sub>5</sub><sup>2+</sup>-ZSM-5 upon exposure to CH<sub>4</sub> at 950 K for 1 h (Fig. 10). These features can be described with the use of a cluster with three Mo–C shells and a total coordination of 3.4 together with a weak contribution from a Mo–Mo shell at 0.29 nm with a coordination number of 0.3. A new feature near 0.12 nm appeared in the radial structure function after exposure to CO<sub>2</sub>/CH<sub>4</sub> mixtures at 950 K for 1 h (Fig. 10), but the sample otherwise retained the features present in the sample during contact with pure CH<sub>4</sub> reactants. The fea-

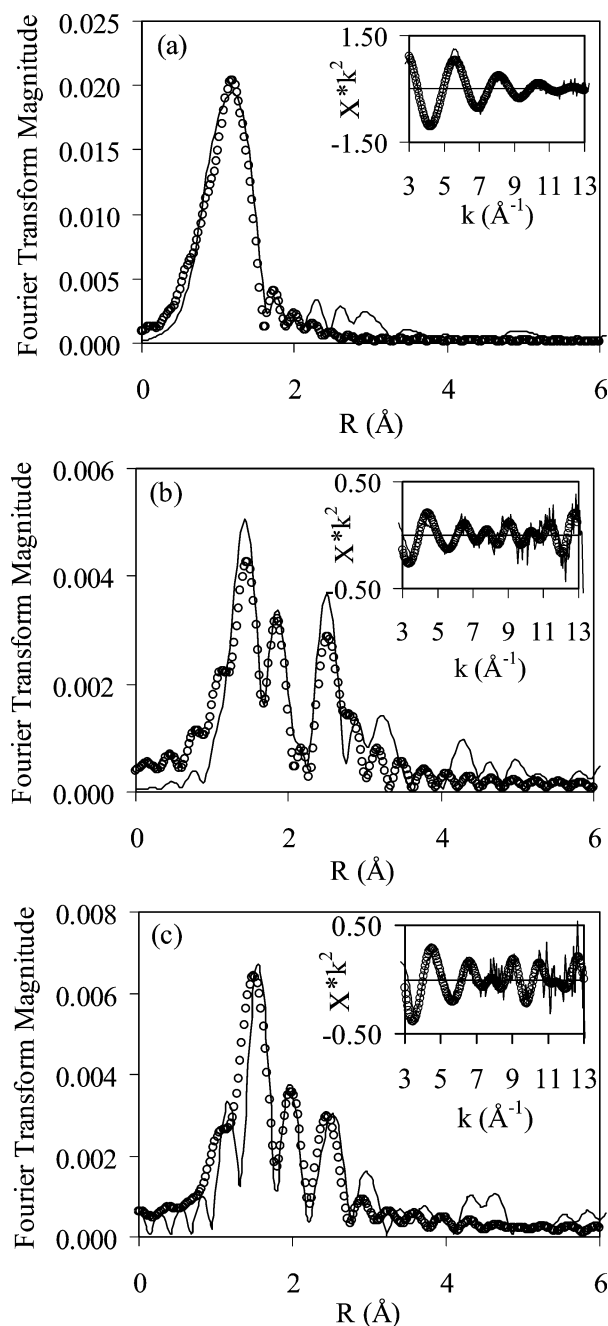


Fig. 10. Multiple scattering fit (circles) to Fourier-transformed  $k^2$ -weighted EXAFS for exchanged Mo/H-ZSM-5 (Mo/Al<sub>F</sub> = 0.41, 950 K): (a) in 20% O<sub>2</sub>/He, (b) carburized 1 h in CH<sub>4</sub>, and (c) treated in a mixture with 0.025 CO<sub>2</sub>/CH<sub>4</sub> for 1 h after (b). Insets show  $k^2$ -weighted EXAFS region. Solid lines in insets represent experimental data and circles represent fit.

ture at 0.12 nm and the rest of the radial structure function resemble those in bulk Mo<sub>2</sub>C containing some oxygen coordination as a result of exposure to ambient air (Fig. 9). The new feature at 0.12 nm was fitted with a Mo–O shell at 0.17 nm with a coordination number of 0.2. Only two Mo–C shells were needed to describe the structure; this gave an overall Mo–C coordination of 3.4. The Mo-ZSM-5 catalysts in CH<sub>4</sub> and CO<sub>2</sub>–CH<sub>4</sub> lack scattering centers at longer distances, which is typical of the bulk carbide (Fig. 9), sug-

Table 5  
Refined structural parameters for Mo/H-ZSM-5 with different treatments

Mo/H-ZSM-5 treatment	Shell	Coordination number <sup>a</sup> , this study	Interatomic distance (nm), this study	Coordination number <sup>b</sup> , Ref. [19]	Interatomic distance (nm), Ref. [19]
20% O <sub>2</sub> /He	Mo–O	1.0	0.17	1.0	0.169
	Mo–O	1.0	0.17	1.0	0.169
	Mo–O	1.0	0.18	1.0	0.178
	Mo–O	1.0	0.18	1.0	0.184
CH <sub>4</sub>	Mo–C	1.7	0.20	–	–
	Mo–C	1.5	0.23	–	–
	Mo–C	0.2	0.24	–	–
	Mo–Mo	0.3	0.29	–	–
CO <sub>2</sub> /CH <sub>4</sub> = 0.025	Mo–O	0.2	0.17	–	–
	Mo–C	1.9	0.21	–	–
	Mo–C	1.5	0.23	–	–
	Mo–Mo	0.2	0.28	–	–

<sup>a</sup>  $S_0^2 = 0.77$ , Debye–Waller factor fixed at zero, fit using  $k^2$ -weighted EXAFS.

<sup>b</sup>  $S_0^2 = 0.63$ , Debye–Waller factor fixed at zero, fit using  $k^1$ -weighted EXAFS.

gesting the presence of small clusters of a size similar to that found with those samples exposed to pure CH<sub>4</sub> reactants.

In Fig. 11, the time evolution of Mo structures obtained from principal component analyses of near-edge spectra is shown together with the amount of extraframework oxygen as measured by mass spectrometry as the composition of the reactant stream was varied with time. In the left panel, fresh Mo<sub>2</sub>O<sub>5</sub><sup>2+</sup>-ZSM-5 was exposed to a 50% CH<sub>4</sub>/He stream (1 bar, 950 K; 5.8 cm<sup>3</sup> s<sup>-1</sup> g<sub>cat</sub><sup>-1</sup>) within the X-ray absorption reactor cell and within a laboratory reactor in separate experiments. The data shown represent the fraction of the Mo atoms present as Mo<sub>2</sub>O<sub>7</sub><sup>2-</sup> and MoC<sub>x</sub>, calculated with the use of MgMo<sub>2</sub>O<sub>7</sub> and bulk Mo<sub>2</sub>C near-edge spectra as standards for the near-edge spectral analysis. Changes in the number of O atoms removed coincided with changes in the local coordination and the oxidation state of Mo atoms measured from near-edge spectra.

After catalysts were fully carburized, the reactant stream was changed to a CO<sub>2</sub>/CH<sub>4</sub> mixture with a ratio of 0.025 (shown in the right panel). Here again, changes in the near-edge spectra occurred within the same time scale as the addition of O atoms measured by mass spectrometry (the initial lag in the change in MoO<sub>x</sub> phase measured from X-ray absorption reflects differences in the time required for the new stream to reach the sample). After approximately 2.5 ks, the oxidation of MoC<sub>x</sub> clusters stops and CO<sub>2</sub>–CH<sub>4</sub> reforming near the bed inlet and CH<sub>4</sub> pyrolysis near the bed outlet reach steady-state rates. These data do not allow unequivocal structural identification because the predominant Mo phase changes with CO<sub>2</sub> concentration along the reactor. The oxidized Mo phase may form precursor-like Mo<sub>2</sub>O<sub>5</sub><sup>2+</sup> species at sufficiently high CO<sub>2</sub> concentrations or MoO<sub>2</sub> clusters, as also occurs during deactivation of bulk Mo<sub>2</sub>C at stoichiometric CO<sub>2</sub>-reforming feeds [28]. The appearance of a pre-edge feature in the near-edge spectra for Mo-ZSM-5 samples exposed to 0.025 CO<sub>2</sub>/CH<sub>4</sub> reactants (Fig. 8) suggests that Mo<sub>2</sub>C oxidizes to volatile MoO<sub>3</sub> within regions of

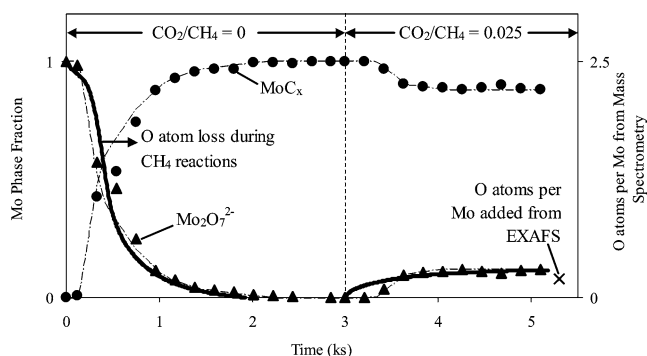


Fig. 11. Mo phase fraction as a function of time on Mo<sub>2</sub>O<sub>5</sub><sup>2+</sup>-ZSM-5 (Mo/Al<sub>F</sub> = 0.41). The Mo phase fraction (denoted with symbols connected with broken lines) was determined using a least square's fit of MgMo<sub>2</sub>O<sub>7</sub> and Mo<sub>2</sub>C near-edge reference spectra to Mo-ZSM-5 catalysts in different oxidizing environments: 50 kPa CH<sub>4</sub> with 0 kPa (left) and 1.3 kPa (right) CO<sub>2</sub> at 950 K, 5.8 cm<sup>3</sup> s<sup>-1</sup> g<sub>cat</sub><sup>-1</sup>. Solid lines indicate O/Mo ratios in the catalyst measured using on-line mass spectrometry (1 g, Mo/Al<sub>F</sub> = 0.41, 950 K, 5.8 cm<sup>3</sup> s<sup>-1</sup> g<sub>cat</sub><sup>-1</sup>, 54 kPa CH<sub>4</sub>) with 0 kPa (left) and 1.2 kPa (right) CO<sub>2</sub>.

the sample containing high enough CO<sub>2</sub> concentrations because MoO<sub>2</sub> has no pre-edge feature. These MoO<sub>3</sub> species would then redisperse to form the Mo-oxo dimers present in the starting material while the rest of the catalyst continues to function as fully carburized clusters active in CH<sub>4</sub> pyrolysis reactions.

#### 4. Conclusions

The improvement in the stability of MoC<sub>x</sub>-ZSM-5 catalysts resulting from the addition of an oxidant such as CO<sub>2</sub> at low concentrations to CH<sub>4</sub> feeds is a result of the H<sub>2</sub> formed by CO<sub>2</sub>–CH<sub>4</sub> reactions. CH<sub>4</sub> reacts with CO<sub>2</sub> exclusively at the beginning of the bed; this reaction occurs via scavenging of surface C\* and inhibits C–C bond formation. After CO<sub>2</sub> is completely consumed, pyrolysis products are formed at



lower yields as a result of H<sub>2</sub> formed in the CO<sub>2</sub>–CH<sub>4</sub> section of the bed; H<sub>2</sub> decreased equilibrium yields to products and increased hydrogenation rates of surface species, preventing formation of carbonaceous deposits that have been linked to catalyst deactivation.

X-ray absorption and transient addition/removal of O atoms during CO<sub>2</sub> addition/removal to CH<sub>4</sub> streams provided strong evidence that Mo was oxidized to MoO<sub>x</sub>C<sub>y</sub>. Oxidized molybdenum carbide clusters formed remained active for CO<sub>2</sub> reforming below CO<sub>2</sub>/CH<sub>4</sub> molar ratios of 0.1. The structure of the catalyst in CO<sub>2</sub>/CH<sub>4</sub> feeds, determined from multiple scattering simulations of the radial scattering function, resembles that of 0.6 nm MoC<sub>x</sub> clusters with a Mo–O coordinative shell at 0.17 nm. At CO<sub>2</sub> concentrations above 0.1 CO<sub>2</sub>/CH<sub>4</sub>, the catalyst became inactive, apparently the result of molybdenum oxide formation, but catalytic activity was restored in pure CH<sub>4</sub> after the removal of oxygen added during CO<sub>2</sub>/CH<sub>4</sub> feeds.

## Acknowledgments

The authors acknowledge the assistance of Dr. Félix Requejo with the collection and analysis of X-ray absorption data. Portions of this research were carried out at the Stanford Synchrotron Research Laboratory, a national user facility operated by Stanford University on behalf of the US Department of Energy, Office of Basic Energy Sciences. The authors acknowledge partial support by BP as part of the Berkeley-Caltech Methane Conversion Cooperative Program under the stewardship of Dr. Theo Fleisch. Howard Lacheen acknowledges with thanks the financial support of the Ford Corporation through the Ford Catalysis Fellowship administered by the Berkeley Catalysis Center.

## References

- [1] F. Kapteijn, G. Marban, J. Rodriguez-Mirasol, J.A. Moulijn, *J. Catal.* 167 (1997) 256.
- [2] T. Mole, J.R. Anderson, G. Creer, *Appl. Catal.* 17 (1985) 141.
- [3] S.N. Bulford, E.E. Davies, US Patent 4,157,356 (1979).
- [4] R. Gregory, A.J. Kolombos, US Patent 4,056,575 (1977).
- [5] M.S. Scurrall, *Appl. Catal.* 41 (1988) 89.
- [6] Y. Ono, K. Kanae, *J. Chem. Soc., Faraday Trans.* 87 (1991) 663.
- [7] R. Shigeishi, A. Garforth, I. Harris, J. Dwyer, *J. Catal.* 130 (1991) 423.
- [8] M. Guisnet, N.S. Gnep, D. Aittaleb, J.Y. Doyemet, *Appl. Catal.* 87 (1992) 255.
- [9] H. Kitagawa, Y. Sendoda, Y. Ono, *J. Catal.* 101 (1986) 12.
- [10] G.L. Price, V.I. Kanazirev, *J. Catal.* 126 (1990) 267.
- [11] Y. Ono, K. Kanae, *J. Chem. Soc., Faraday Trans.* 87 (1991) 669.
- [12] K.M. Dooley, G.L. Price, V.I. Kanazirev, V.I. Hart, *Catal. Today* 31 (1996) 305.
- [13] B.S. Kwak, W.M.H. Sachtler, *J. Catal.* 145 (1994) 456.
- [14] Y. Ono, H. Kitagawa, Y. Sendoda, *J. Chem. Soc., Faraday Trans. I* 89 (1987) 2913.
- [15] L. Wang, L. Tao, M. Xie, G. Xu, *Catal. Lett.* 21 (1993) 35.
- [16] D. Wang, J.H. Lunsford, M.P. Rosynek, *Top. Catal.* 3 (1996) 289.
- [17] R.W. Borry, Y.-H. Kim, A. Huffsmith, J.A. Reimer, E. Iglesia, *J. Phys. Chem. B* 103 (1999) 5787.
- [18] Y.-H. Kim, R.W. Borry, E. Iglesia, *Micropor. Mesopor. Mater.* 35 (2000) 495.
- [19] W. Li, G.D. Meitzner, R.W. Borry, E. Iglesia, *J. Catal.* 191 (2000) 373.
- [20] F. Solymosi, A. Erdöhelyi, A. Szöke, *Catal. Lett.* 32 (1995) 43.
- [21] B.M. Weckhuysen, D.J. Wang, M.P. Rosynek, J.H. Lunsford, *J. Catal.* 175 (1998) 338.
- [22] Y. Shu, H. Ma, R. Ohnishi, M. Ichikawa, *Chem. Commun.* (2003) 86.
- [23] W. Ding, G.D. Meitzner, E. Iglesia, *J. Catal.* 206 (2002) 14.
- [24] R. Ohnishi, S. Liu, Q. Dong, L. Wang, M. Ichikawa, *J. Catal.* 182 (1999) 92.
- [25] Y. Shu, R. Ohnishi, M. Ichikawa, *J. Catal.* 206 (2002) 134.
- [26] Z. Liu, M.A. Nutt, E. Iglesia, *Catal. Lett.* 81 (2002) 271.
- [27] B.M. Weckhuysen, M.P. Rosynek, J.H. Lunsford, *Catal. Lett.* 52 (1998) 31.
- [28] J.B. Claridge, A.P.E. York, A.J. Brungs, C. Marquez-Alvarez, J. Sloan, S.C. Tsang, M.L.H. Green, *J. Catal.* 180 (1998) 85.
- [29] H.S. Lacheen, E. Iglesia, *Phys. Chem. Chem. Phys.*, in press.
- [30] M. Boudart, G. Djega-Mariadassou, *Kinetics of Heterogeneous Catalytic Reactions*, Princeton University Press, Princeton, NJ, 1984.
- [31] G.D. Meitzner, E. Iglesia, *Catal. Today* 53 (1999) 433.
- [32] D.G. Barton, S.L. Soled, G.D. Meitzner, G.A. Fuentes, E. Iglesia, *J. Catal.* 181 (1999) 57.
- [33] J.S. Lee, S.T. Oyama, M. Boudart, *J. Catal.* 106 (1987) 125.
- [34] K. Stadnicka, *Acta Cryst. B* 33 (1977) 3859.
- [35] WinXAS, v. 2.1 licensed by T. Ressler, Fritz Haber Institut der MPG, Dept. of Inorganic Chem., Faradayweg 4-6, D-14195, Berlin, Germany (email: [t\\_ressler@winxas.de](mailto:t_ressler@winxas.de)).
- [36] M. Newville, B. Ravel, D. Haskel, J.J. Rehr, A. Stern, Y. Yacoby, *Physica B* 208 (1995) 154.
- [37] J.J. Rehr, R.C. Albers, S.I. Zabinsky, *Phys. Rev. Lett.* 69 (1992) 3397.
- [38] B. Ravel, *J. Synch. Rad.* 8 (2001) 314.
- [39] E.R. Malinowski, *Factor Analysis in Chemistry*, Wiley, New York, 2002.
- [40] T. Ressler, J. Wong, J. Roos, I. Smith, *Environ. Sci. Tech.* 34 (2000) 950.
- [41] Chemkin Collection Software, v. 3.6 licensed by Reaction Design, 6440 Lusk Blvd., Suite D-209, San Diego, CA, 92121.
- [42] D.R. Lide, *CRC Handbook of Chemistry and Physics*, 75 ed., CRC Press, Boca Raton, 1994.
- [43] W.W. Akres, D.P. Camp, *AIChE J.* 1 (1955) 471.
- [44] J. Wei, E. Iglesia, *J. Catal.* 224 (2004) 370.
- [45] W. Ding, S. Li, G.D. Meitzner, E. Iglesia, *J. Phys. Chem. B* 105 (2001) 506.
- [46] D. Ma, D. Wang, L. Su, Y. Shu, Y. Xu, X. Bao (2002).
- [47] T. Ressler, O. Timpe, T. Neisius, J. Find, G. Mestl, M. Dieterle, R. Schlögl, *J. Catal.* 191 (2000) 75.
- [48] T. Ressler, R.E. Jentoft, J. Wienold, M.M. Günter, O. Timpe, *J. Phys. Chem. B* 104 (2000) 6360.
- [49] M.J. Fay, A. Proctor, D.P. Hoffmann, M. Houalla, D.M. Hercules, *Mikrochim. Acta* 109 (1992) 281.
- [50] F.W. Kutzler, C.R. Natoli, D.K. Misemer, S. Doniach, K.O. Hodgson, *J. Chem. Phys.* 73 (1980) 3274.
- [51] M. Fernández-García, C.M. Alvarez, G.L. Haller, *J. Phys. Chem.* 99 (1995) 12565.
- [52] S.R. Wasserman, *J. Phys. IV* 7 (1997) 203.